International Journal of Mechanical, Industrial and Aerospace Sciences
ISSN: 2517-9950
Vol:12, No:6, 2018

Compressible Flow Modeling in Pipes and Porous Media during Blowdown Experiment

Thomas Paris, Vincent Bruyere, Patrick Namy

Abstract**—**A numerical model is developed to simulate gas blowdowns through a thin tube and a filter (porous media), separating a high pressure gas filled reservoir to low pressure ones. Based on a previous work, a one-dimensional approach is developed by using the finite element method to solve the transient compressible flow and to predict the pressure and temperature evolution in space and time. Mass, momentum, and energy conservation equations are solved in a fully coupled way in the reservoirs, the pipes and the porous media. Numerical results, such as pressure and temperature evolutions, are firstly compared with experimental data to validate the model for different configurations. Couplings between porous media and pipe flow are then validated by checking mass balance. The influence of the porous media and the nature of the gas is then studied for different initial high pressure values.

Keywords**—**Fluid mechanics, compressible flow, heat transfer, porous media.

I. Introduction

THE correct assessment of gas behavior is of paramount importance in the design procedure of pipes and reservoirs in gas industry. To this end, a numerical modelling strategy of the gas behavior during a blowdown experiment is developed in this paper. The main objective is to develop a simplified yet accurate model that will enable the prediction of the pressure and temperature evolution during a depressurization process. This will allow an optimized design of the pipes and reservoirs as well as the monitoring of the time required to reach thermodynamic equilibrium during technical incident. However, due to high pressure gradients occurring in the flow, the gas velocity is locally equal to the sound velocity. The subsequent flow is then highly transient, turbulent and compressible. Modeling such flow can be very complex and requires important computational time. In order to obtain a simplified and fast model, the choice of different assumptions is crucial and a careful validation is required.

A first step of the model has been presented and numerically validated in previous works [1]. The numerical pressure evolution predictions were compared with experimental data. Discrepancies between the two approaches were identified and accounted for by inaccuracies in temperature measurements. Indeed, due to very fast temporal variations occurring in the process, the response of the sensors should be upgraded to capture these phenomena. To improve the knowledge and confidence in the model assumptions, an extension of the modeling to the full experimental system is henceforth taken into account. Moreover, the influence of a porous media, as well as the nature of the gas is studied in this work.

An overview of the system is given in Fig. 1. It is formed of three spherical reservoirs: the container (C) and two receivers (R_1) and (R_2). A porous media (PM) is added and its influence will be studied hereafter. The container is initially set at high pressure and is separated by a valve V_1 from the others. Both low pressure reservoirs (R_1) and (R_2), exhibiting potentially different volumes, are isolated by two valves V_2 and V_3. All the reservoirs and the porous media are connected by a pipe network (P) of constant section and filled with gas.

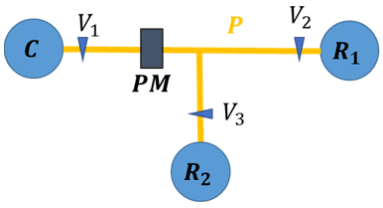

Fig. 1 Overview of the system

After a description of modeling assumptions and resulting equations, numerical aspects will be discussed. Numerical results will then be analyzed and confronted with experimental measurements for three process configurations.

II. Modeling

Given the complexity of the flow, several assumptions are used to simplify the problem starting with the geometry. Due to the dimensions of the pipes (P), i.e. the high ratio between their length and their diameter, a one-dimensional approach is adopted. The velocity profile is fully developed through the pipe section, and curvature of the pipes leads to insignificant pressure loss. All velocity components normal to the pipe axis are thus assumed to be null. The same assumption is used regarding the porous media (PM) due to high pressure gradients. The reservoirs (C), (R_1) and (R_2) are geometrically reduced to points as they are large comparing to the tube section. The gas velocity is considered negligible therefore temperature and pressure fields can be assumed uniform. The resulting equations are presented for each component in the following paragraphs.

A. In the Pipe Network

In the pipe network (P), four equations are used to describe the compressible flow. Equations (1)-(3) refer to the mass,

T. Paris is with the CEA DAM, Valduc, Is-sur-Tille, France (e-mail: thomas.paris@cea.fr).
V. Bruyere and P. Namy are with SIMTEC, 8, rue Duploye, 38100, Grenoble, France.

momentum and energy balance respectively. Equation (4) is the ideal gas law:

$$\frac{\partial \rho}{\partial t} + \nabla_t \cdot (\rho u \boldsymbol{e_t}) = 0 \quad (1)$$

$$\rho \left(\frac{\partial u}{\partial t} + u \nabla_t \cdot (u \boldsymbol{e_t}) \right) = -\nabla_t p \cdot \boldsymbol{e_t} - \frac{\rho}{2 d_h} f_D |u| u \quad (2)$$

$$\rho C_p \left(\frac{\partial T}{\partial t} + u \boldsymbol{e_t} \cdot \nabla_t T \right) = \nabla_t \cdot (k \nabla_t T) + \frac{\rho}{2 d_h} f_D |u| u^2 + \frac{\partial p}{\partial t} + u \boldsymbol{e_t} \cdot \nabla_t p \quad (3)$$

$$\rho = \frac{pM}{RT} \quad (4)$$

where ρ is the density, u is the velocity, p is the pressure, T is the temperature, $\boldsymbol{e_t}$ is the unit tangent vector to the pipe axis, d_h is the mean hydraulic diameter, f_D is the Darcy friction factor, C_p is the heat capacity at constant pressure, k is the conductivity, M is the molar mass, and R is the ideal gas constant.

As proposed in [1], a global friction factor, f_D , can be used to describe the friction losses as a function of the rugosity of the pipe and of the Reynolds number. It is given by the *Churchill's friction model* [2] which can be used both in laminar, transition and turbulent regimes which are reached in the process. During the process, the second law of thermodynamics imposes that the Mach number, $Ma = \frac{u}{\sqrt{\gamma \frac{R}{M} T}}$ (with γ the ratio of specific heats), within the pipe cannot exceed a value of 1 since the section is constant [3]. To respect this constraint, the approach detailed in [1] is adopted for sonic flow conditions at the junction between pipes and reservoirs (R_1) and (R_2).

B. In the Reservoirs

In the reservoirs (C), (R_1) and (R_2), the gas satisfies the mass and energy balances, and the ideal gas law. Since the pressure in (C) is higher than in the rest of the system, when the valve is opened the container empties and transfers mass and kinetic energy to the pipe. Symmetrically, (R_1) and (R_2) gain mass and energy during the discharge. All the vessels exchange heat with their environment. This is modeled with convective exchange coefficients h_W^C and $h_W^{R_i}$. Equations (5) and (6) describe the resulting mass and energy balances:

$$V^C \frac{\partial (\rho^C T^C)}{\partial t} = -\rho u A \quad (5)$$

$$C_v V^C \frac{\partial (\rho^C T^C)}{\partial t} = -\rho u A \left(C_p T + \frac{u^2}{2} \right) + h_W^C S^C (T^E - T^C) \quad (6)$$

with V^C is the volume, S^C is the section, ρ^C is the density, T^C is the temperature of the container, and C_v is the heat capacity at constant volume, A is the pipe section and T^E is the ambient temperature.

In the reservoirs (R_1) and (R_2), mass and energy balances are expressed as:

$$V^{R_i} \frac{\partial \rho^{R_i}}{\partial t} = \rho u A \quad (7)$$

$$C_v V^{R_i} \frac{\partial (\rho^{R_i} T^{R_i})}{\partial t} = \rho u A \left(C_p T + \frac{u^2}{2} \right) + h_W^{R_i} S^{R_i} (T^E - T^{R_i}) \quad (8)$$

with V^{R_i} is the volume, S^{R_i} is the section, ρ^{R_i} is the density, T^{R_i} is the temperature of the receiver (R_i) $(i = 1\ to\ 2)$.

As proposed in [4], the modelling can be simplified by expressing exchange coefficients for each receiver through a function of non-dimensional numbers. The exchange coefficients, h_W (for each container), are split between one coefficient linked to natural convection, h_{NC}, and one related to forced convection h_{FC}:

$$h_W = \alpha h_{NC} + \beta h_{FC} \quad (9)$$

The first one is expressed by:

$$h_{NC} = k \frac{Nu}{r} \quad (10)$$

with r, the radius of the reservoir and Nu, the Nusselt number, defined by:

$$Nu = \begin{cases} 0.1 * Ra^{0.33} & if\ Ra > 10^9 \\ 0.47 * Ra^{0.25} & if\ Ra \leq 10^9 \end{cases} \quad (11)$$

with Ra the Rayleigh number:

$$Ra = \frac{g (T^E - T) \rho^2 r^2 C_p}{k \eta T} \quad (12)$$

with g, the standard gravity constant.

Concerning the forced convection, the exchange coefficient is defined by:

$$h_{FC} = 0.023 * Re^{0.8} Pr^{0.33} \quad (13)$$

with $Re = \frac{\rho d_h u}{\eta}$, the Reynolds number and $Pr = \frac{C_p \eta}{k}$, the Prandtl number.

The values of α and β in (9) are obtained from previous studies and are identical for each configuration studied hereinafter.

C. In the Porous Media

Flowing through the porous media causes the pressure to drop in the fluid because of the viscous effects and the resistance of the media. The Darcy law is used to compute the velocity from the pressure gradient (assumed to be one-dimensional):

$$u = -\frac{\kappa}{\eta} \nabla p \quad (14)$$

with κ is the permeability of the media and η is the gas viscosity.

The continuity equation is solved in the pore volume to obtain the transient evolution of the pressure field:

$$\frac{\partial}{\partial t}(\varepsilon\rho) + \nabla \cdot (\rho u) = 0 \quad (15)$$

with ε is the porosity, ρ is the density obtained from the ideal gas law (4) and u is the velocity obtained from (14).

Several empiric laws can be derived to express the permeability as a function of the porosity or the grain size. In this work, the Kozeny-Carman formulation [5], [6] is used to link the permeability coefficient with the porosity and the specific surface area of the porous media:

$$\kappa = \frac{\varepsilon^3}{5S_{spec}^2(1-\varepsilon)^2} \quad (16)$$

with $S_{spec} = \frac{6}{d_g}$ the specific surface area obtained from the grain size of the porous media d_g.

To evaluate the gas viscosity, the Sutherland's relationship is used for each considered gas [7]:

$$\eta = \eta_0 \left(\frac{T}{T_0}\right)^n \quad (17)$$

with η_0 the reference viscosity at the reference temperature T_0 and $n = 0.68$.

The porous media is described by an equivalent domain in the energy balance. The effective volumetric heat capacity, $(\rho C_p)_{eff}$, as well as the thermal conductivity k_{eff}, is defined by an averaging model which accounts for both solid matrices (subscripted by s in (18)) and fluid. The convective term is only linked to the fluid properties. The following equation is solved to obtain the temperature evolution in the porous media:

$$(\rho C_p)_{eff}\frac{\partial T}{\partial t} + \rho C_p u \nabla T = \nabla \cdot (k_{eff}\nabla T) \quad (18)$$

with $(\rho C_p)_{eff} = \varepsilon\rho C_p + (1-\varepsilon)\rho_s C_{p_s}$ and $k_{eff} = \varepsilon k + (1-\varepsilon)k_s$.

III. Study Cases and Numerical Aspects

At the beginning of the process, all the valves are closed. The initial pressure is set at a high value, p_0^C, in the container (C) (see Table I) and at ambient pressure elsewhere ($p_0 = 1\ bar$). The initial temperature is set at room temperature in each component.

The first discharge occurs when the valve V_1 is opened followed by V_2, causing the gas flow from (C) to (R_1) through a small diameter orifice. At a given time $\tau = 0.63\ ms$, V_2 is closed and V_3 opened brutally resulting in fulfillment of another tank (R_2) without restriction (same pipe diameter everywhere). In order to understand the influence of the gas nature (mono and diatomic gas of different molar mass) and the presence of a porous media, three configurations are studied in this work, all following the same scenario. Main differences are summarized in Table I.

To solve this transient and highly coupled problem, the COMSOL Multiphysics® software is used with the finite element method. A direct approach is used to solve the linearized problem with the PARDISO solver and the BDF solver is used for the time-dependent terms [8]. A mesh convergence has been performed to guarantee the validity of the results. The CPU time is roughly 1 minute with a Personal Computer of 4 processors and 16 Go RAM for 2 seconds of process.

TABLE I
Study Cases

Case	Gas Nature	$p_0^C\ (bar)$	Presence of (PM)
A	H_2	147	*No*
B	^4He	175	*No*
C	^4He	190	*Yes*

An example of the mass conservation in the model is shown in Fig. 2. The mass flow evolution is plotted as a function of the abscissa upstream and downstream the porous media (PM) for three different instants (at the top, Fig. 2). It is shown that between each junction between pipes and (PM) (color variations, at the top, Fig. 2), mass flow is conserved. By analyzing the mass flow evolution in each receiver (at the bottom, Fig. 2), same values are obtained for these three instants, validating the numerical couplings.

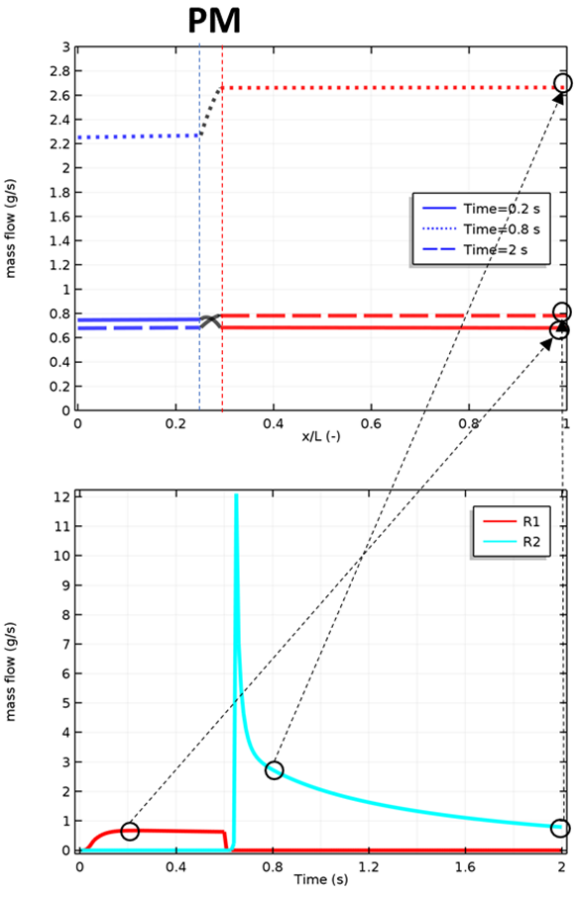

Fig. 2 Mass flow evolution as a function of space between the different components (in downstream and upstream of (PM)) at three different instants: $t = 0.2$ s, $t = 0.8$ s, $t = 2$ s (at the top) and mass flow evolution as a function of time in (R_1) and (R_2) (at the bottom)

IV. Experimental Comparison and Validation

To validate this numerical approach, an experimental study of the process was performed. As introduced in Section III, the experimental process has two steps, leading to the filling of two receivers (R_1) and (R_2). Each component is instrumented with pressure and temperature transducers in order to record quantities during the whole process. In a previous paper [1], only the second part of the process was discussed and modeled. A shift in the pressure in (R_2) was observed during each experiment considered. In fact, the quantity of gas in (C), i.e. its mass, seemed to be underestimated. It was explained by an inaccurate measurement of the temperature and in particular of the initial temperature. In reality, in the experiments, a first discharge occurs from (C) resulting in the absence of an equilibrium starting point.

The improvement of the two-step modeling is now discussed and compared with additional experimental tests.

A. Transient Temperature and Heat Exchange Coefficient Identification in (R_1)

To allow to discuss this point in depth, the explicit simulation of the first step was undertaken and then switch from (R_1) to (R_2) (case A). Before switching ($t < 0.63s$, Fig. 3), experimental and simulated data are in good agreement, but experimental temperature is delayed as mentioned earlier.

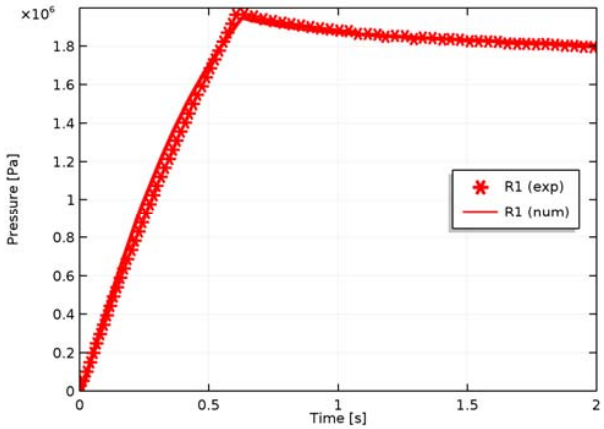

Fig. 3 Pressure difference comparison (without the porous media) in (R_1) between experimental and simulated data

After switching, (R_1) is closed and the transient temperature can be calculated by recording experimentally pressure relaxation to equilibrium (Fig. 4).

The knowledge of the temperature values during the transient state enabled the identification of the heat exchange coefficient which provided the best result during relaxation process in (R_1) as it can be seen in Figs. 3 and 4. Mass flow rate is nearly constant during choked flow and then decreases due to pressure drop in (C) and pressure rise in (R_1) (this can be seen in Fig. 5 through velocity and Mach number evolutions). The choked flow condition in the orifice is thus well managed, validating this approach.

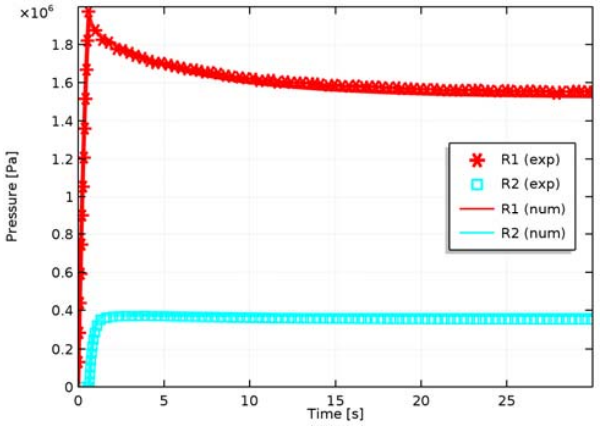

Fig. 4 Pressure difference comparison in (R_1) between experimental and simulated data: return to equilibrium

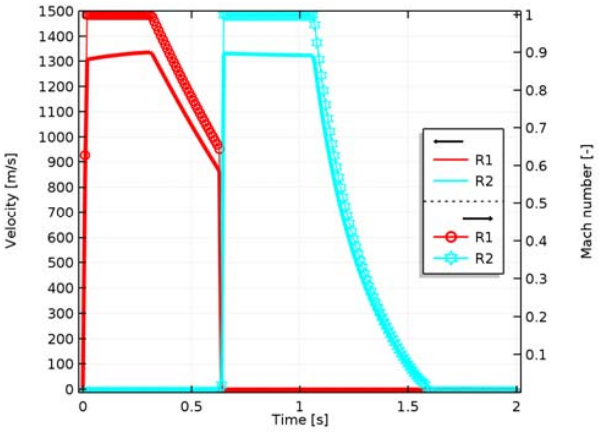

Fig. 5 Velocity (on the left) and Mach number (on the right) at the junction between the pipe and (R_1) and between the pipe and (R_2)

At this stage, there are no other fitting parameters than heat exchange coefficients in (C) and (R_1). Another interesting correlation showing physical strong description of choked flow, is given by the filling of (R_2) after switching. During this stage, gas flows directly through the pipe without orifice showing that choked flow condition is well managed for different pipe diameters.

B. Pressure Drop in (C)

Consequently, pressure drop in (C) also exhibits a two-slope curve (Fig. 6). The first stage before switching is a slow discharge through an orifice in (R_1) (the smallest volume reservoir), and the second stage is a fast discharge directly to (R_2) (high volume reservoir).

As mentioned earlier, pressure drop in (C) reveals a good description of the mass flow rate in (R_1) and (R_2) and also a good correlation with temperature drop due to gas expansion process. The identification of the heat exchange coefficient to take into account the exchange with the environment during the temperature decrease (Fig. 7) is performed as described for (R_1) and (R_2). Moreover, it is interesting to mention that this only fitting parameter is kept constant during the two stages

showing the ability to describe different pressure and temperature drop kinetics with the model.

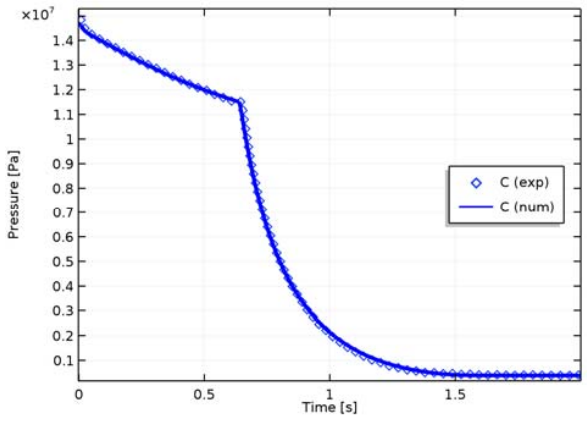

Fig. 6 Pressure comparison in (C) between experimental and simulated data before and after switching

Numerical robustness of the implementation in COMSOL Multiphysics® software can be seen at the exact switching time. Indeed, this crucial time exhibits really sharp changes in boundary conditions for the two vessels and is, consequently, a really strenuous effort for the convergence to be achieved.

C. Temperature Evolutions

The validation of the temperature evolution can be a challenging task for several reasons. The first one has already been discussed and is related to the identification of heat exchange coefficients. The second one has to deal with the model dimension. The reservoirs are modeled in 0-D to improve convergence and computational costs. As no spatial information is required, it seems relevant to use this hypothesis. However, it is implicitly requested that the temperature is quasi uniform which is not the case during transient flow especially for big reservoir ((R_2) for instance). The third reason is related to the experimental measurement itself. The temperature transducers timeframe capability are not sufficient enough to capture fast evolutions and are never really isolated from environment due to inertial effects.

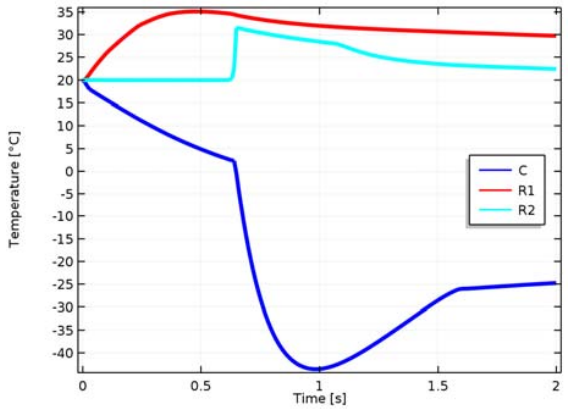

Fig. 7 Temperature evolution in each component: (C), (R_1) and (R_2)

Consequently, temperature measurements are used mainly as indications concerning maximum and minimum reached temperature but cannot be directly compared with simulation due to slow experimental evolutions (Fig. 7).

V. Influence of the Nature of Gas (Case B)

In this experiment, the gas nature is changed from H_2 to ^4He resulting in noticeable changes in flow (mainly due to the change in molar mass and viscosity) and heat conditions (due to the conductivity, heat capacity and a set of dimensionless numbers such as Nusselt, Prandtl, Reynolds, Rayleigh numbers between the two gases).

Compared to the previous experiment (case A), the only modifications are inlet and outlet pressures (from around 150 bars to 175 bars and 70 bars to 40 bars respectively) in conjunction with gas nature.

As can be seen in Fig. 8, the gas flow is really different from case A (Fig. 5). The flow is choked during the whole first step and then the gas velocity slows down slowly in (R_2) compared to case A.

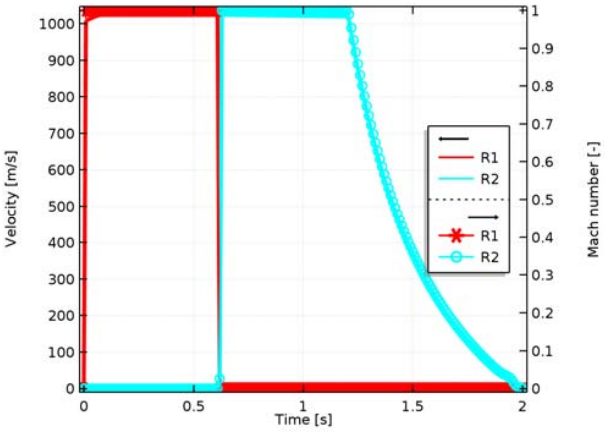

Fig. 8 Velocity (on the left) and Mach number (on the right) at the junction between the pipe and (R_1) and between the pipe and (R_2) for case B

In Fig. 9, the pressure model predictions and experimental results are compared. It can be noticed that even though the flow varies significantly between (R_1), (R_2) and (C), the respective pressure evolutions are very well captured by the model. More specifically, it can be seen that during the first step, the pressure drop in (C) and pressure increase in (R_1) are in good agreement with the experimental results during the whole time period τ. The prediction of the maximum and relaxation pressures after switching in (R_1) is also in good agreement with the experimental results, highlighting that temperature is also well managed for a fixed set of heat exchange coefficients. However, during the transient process, the predicted pressure in (R_2) exhibits a slight difference compared to that from experimental data. This could be due to a non-equilibrium state between forced and natural convection in the model for a high size tank as (R_2) when the nature of the gas changes. This could be fine-tuned by adjusting the heat

exchange coefficients ratio (forced over natural convection) by adding a relaxation pressure step in (R_2) by closing V_3.

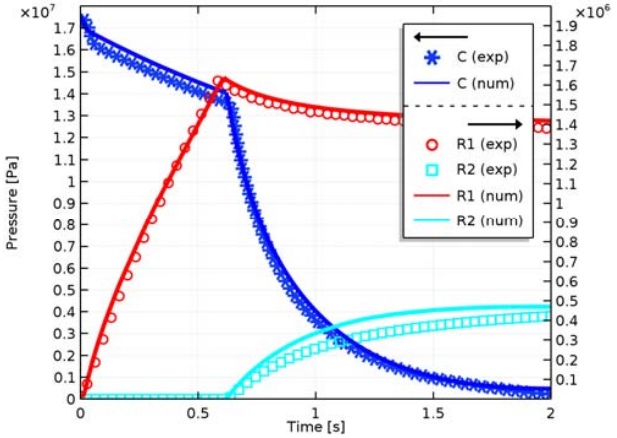

Fig. 9 Pressure comparison in (C) (left scale) and pressure difference comparison in (R_1) and (R_2) (right scale) between experimental and simulated data for case B

VI. Influence of the Filter (Case C)

In this experiment, the nature of the gas is kept constant (^4He) and inlet and outlet pressures roughly also (around 190 bars instead of 175 bars for (C) in case B). The main and significant difference is the addition of a porous media (PM) directly after (C). This influences both the flow in (R_1) but also in (R_2). The low permeability is known and calculated from (16). Additional transducers record porous media pressure inlet and outlet quantifying pressure drop due to the low permeability.

It is possible to distinguish three steps from the results presented in Fig. 10. The first one results from the filter through process (around 50 ms), the second one is the fulfillment of (R_1) with a delay in time caused by the previous step and the third and last one is the fulfillment of (R_2) after switching τ (around 650 ms).

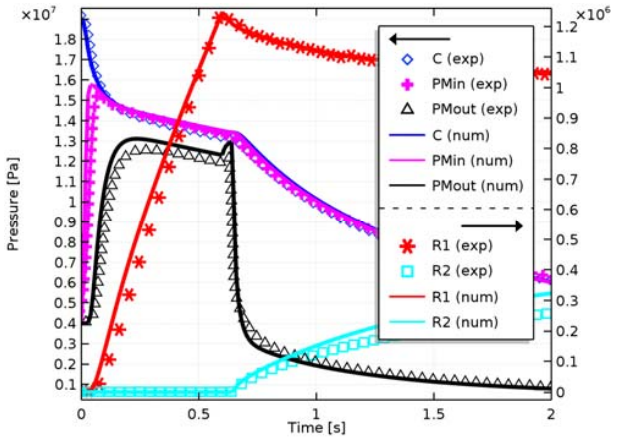

Fig. 10 Pressure comparison in each component: (C), (PM) (in and out), and pressure difference comparison in (R_1) and (R_2)

By keeping every model parameters constant from cases A and B (only input data for different experimental conditions were changed), the model predictions fit remarkably well the experimental test case C results. Even for the updated configurations (inlet and outlet porous media pressure), the agreement is very satisfactory. It can be noticed that the overshoot, at the end of the first step is captured and the pressure drop is also well described even if the outlet porous media pressure is slightly overestimated. At the end of the second step, an interesting feature can be observed on the outlet porous media pressure. The overshoot is caused by valves switching sync and can be simulated by introducing a delay in time corresponding to valve responses (around 30 ms). As it was observed in case B experiment (Fig. 9), the pressure in (R_1) after switching is well captured but slightly overestimated in (R_2) for the same reasons.

As explained earlier, experimental temperature measurement at this timescale is complex and has to be improved for a direct comparison. However, the calculated temperature evolutions in (C) for both cases B and C can be discussed. First of all, it should be highlighted that the evolution in temperatures presented in Fig. 11 clearly exhibits a three-step evolution.

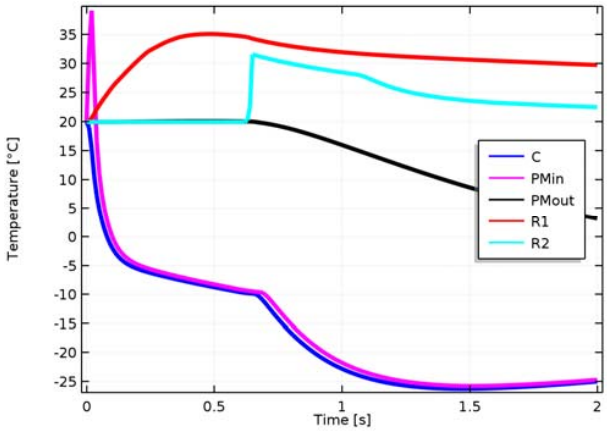

Fig. 11 Temperature evolution in each component: (C), (PM) (in and out), (R_1) and (R_2)

The first step associates rapid depressurization of (C) to faster cooling in case C than case B. This phenomenon is due to the higher volume available in (PM) when V_1 is opened. During the second step, a pressure and temperature plateau arises around -5 °C and -10 °C induced by (PM) permeability which is naturally not seen in case B. As (PM) influences both (R_1) and (R_2) pressure and temperature evolutions, temperature in (C) in the third step (after switching) is significantly different from case B resulting in a 15 °C higher temperature.

VII. Conclusion

A numerical model has been developed to simulate the gas blowdown of a high-pressurized reservoir through several components: pipe network, filter and receivers. To obtain a

fast yet accurate model, appropriate assumptions have been used to simplify the modeling of this complex thermohydraulic problem. After numerical validations, results have been confronted with experimental measurements for several operating conditions. The influence of the nature of the gas and the presence of a porous media has been highlighted by studying pressure and velocity profiles.

The evolutions of pressure with time in each component have been compared for three study cases. The qualitative and quantitative comparison during the whole process proved to be very satisfactory for each configuration, which validates this approach. The model can now be used to accurately predict the behavior of the gas in several operating conditions. In future works, other natures of gas will be studied and compared with experimental data. An improvement of the thermal sensors will also be involved to validate the temperature predictions.

ACKNOWLEDGMENT

The technical operating on experimental tests presented in this paper was done by N. Bourdon and R. Chevalier which are gratefully acknowledged for this significant work.

REFERENCES

[1] V. Bruyere, T. Paris, F. Viry, P. Namy, Compressible Flow Modeling Occurring in a Depressurization Process, *Proceedings of the 2017 Comsol Conference*, Rotterdam, 2017.
[2] S. W. Churchill, Friction factor equation spans all fluid-flow regimes, 1977, pp. 91-92.
[3] A. Lallemand, Ecoulements monodimensionnels des fluides compressibles, *Techniques de l'ingénieur*, 2014.
[4] S. Charton, V. Blet and J. P. Corriou, A Simplified Model for Real Gas Expansion Between Two Reservoirs Connected by a Thin Tube, vol. 51, 1996, pp. 295-308.
[5] Kozeny J., Uber Kapillare Leitung des Wassers im Boden, *Sitzungsber. Akad. Wiss. Wien*, Vol 136, pp. 271–306, 1927.
[6] Carman P C., *Flow of Gases Through Porous Media*, Butterworths, London, 1956.
[7] Sutherland, W. (1893), "The viscosity of gases and molecular force", Philosophical Magazine, S. 5, 36, pp. 507-531 (1893).
[8] Comsol Multiphysics Reference Manual, 2018.